Integrin-Matrix Clusters Form Podosome-like Adhesions in the Absence of Traction Forces

Cheng-han Yu, Nisha Bte Mohd Rafiq, Anitha Krishnasamy, Kevin L. Hartman, Gareth E. Jones, Alexander D. Bershadsky, Michael P. Sheetz

Supplemental Figures

Figure S1. Differential recruitment of MMP-14 and Tks5 between podosome and invadopodia.

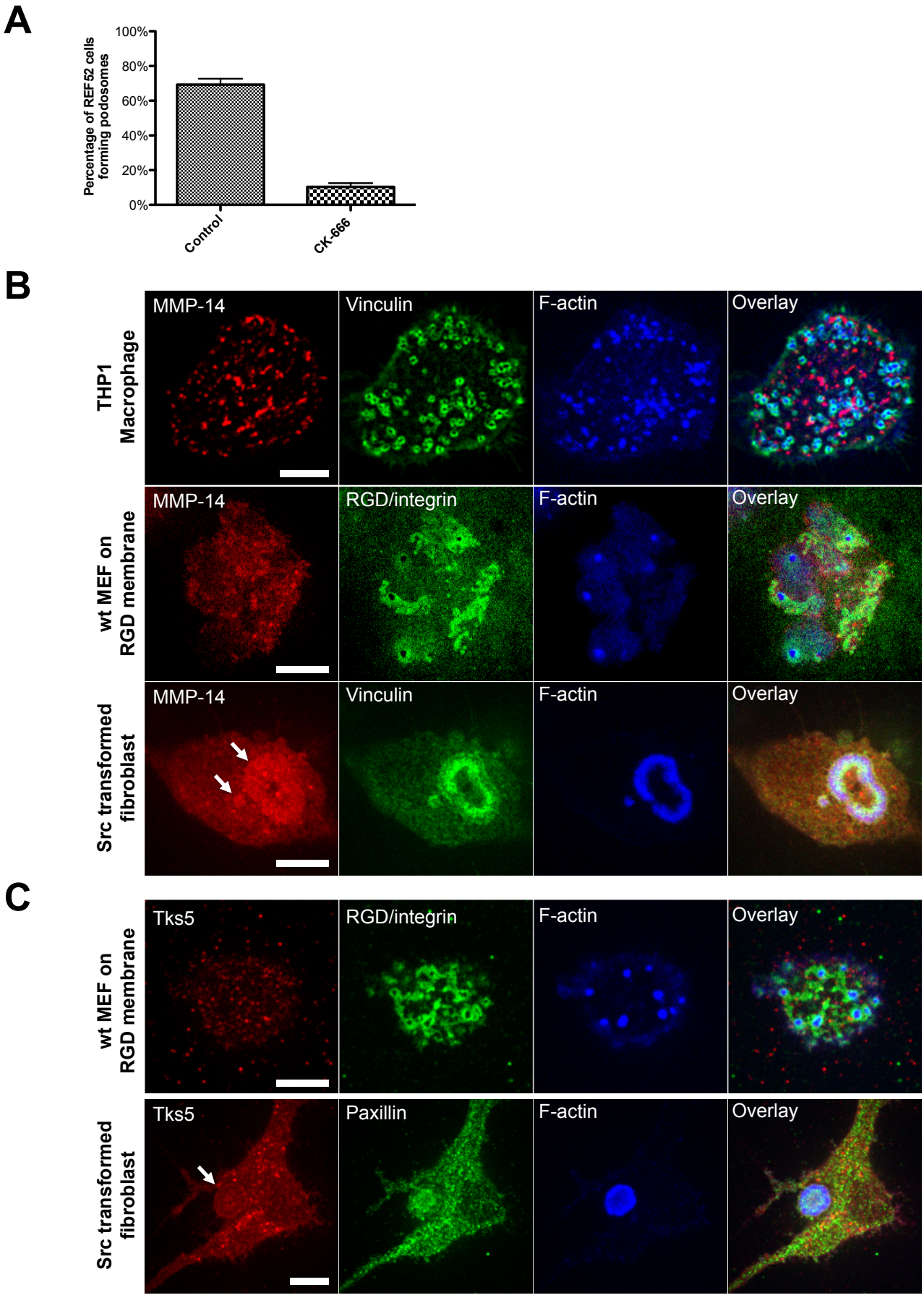

Figure S1. Differential recruitment of MMP-14 and Tks5 between podosome and invadopodia. (A) Arp2/3 inhibitor CK-666 effectively abolished podosome formation. Percentage of REF52 fibroblast cells with CK-666 inhibition forming podosome on RGD-membrane, with SEM from two experiments. REF52 fibroblast cells were pre-incubated with CK-666 (100μM) for 5 hours. Cell was then examined after 1hr of initial adhesion on RGD-membrane. CK-666 effectively inhibited podosome formation. (B) MMP-14 (MT1-MMP) was not recruited at podosomes in both THP1 macrophage and non-transformed fibroblast on RGD membrane. However, MMP-14 was enriched at invadopodia (or long-lived podosomes) in Src-transformed fibroblast. (C) Tks5 was not recruited at podosomes in non-transformed fibroblast, but enriched at invadopodia in Src-transformed fibroblast. Notably, Src-transformed cells exhibit higher expression level of Tks5, while Tks5 level in non-transformed MEF is low. Scale bar 10μm.

Figure S2. Molecular components at podosomes.

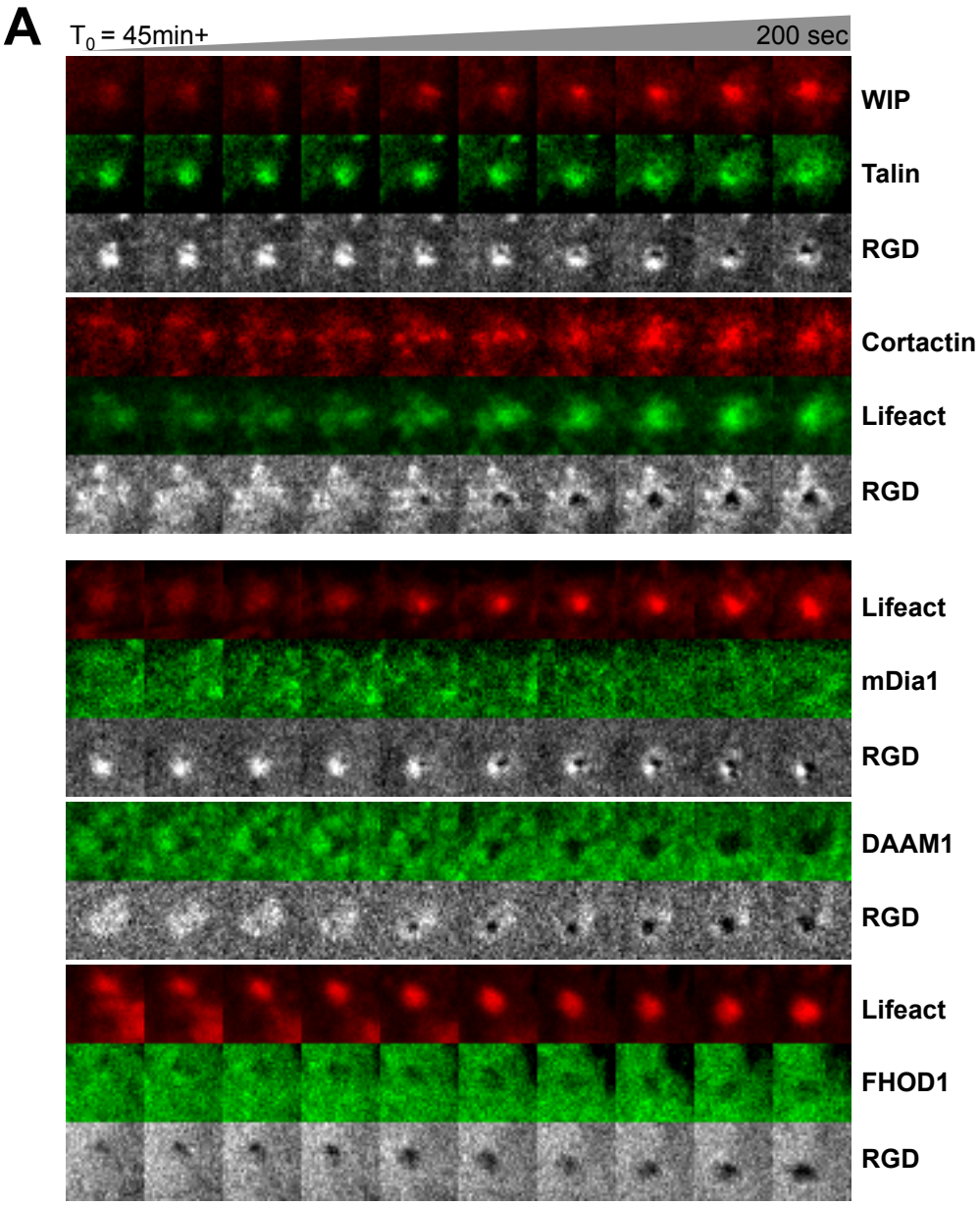

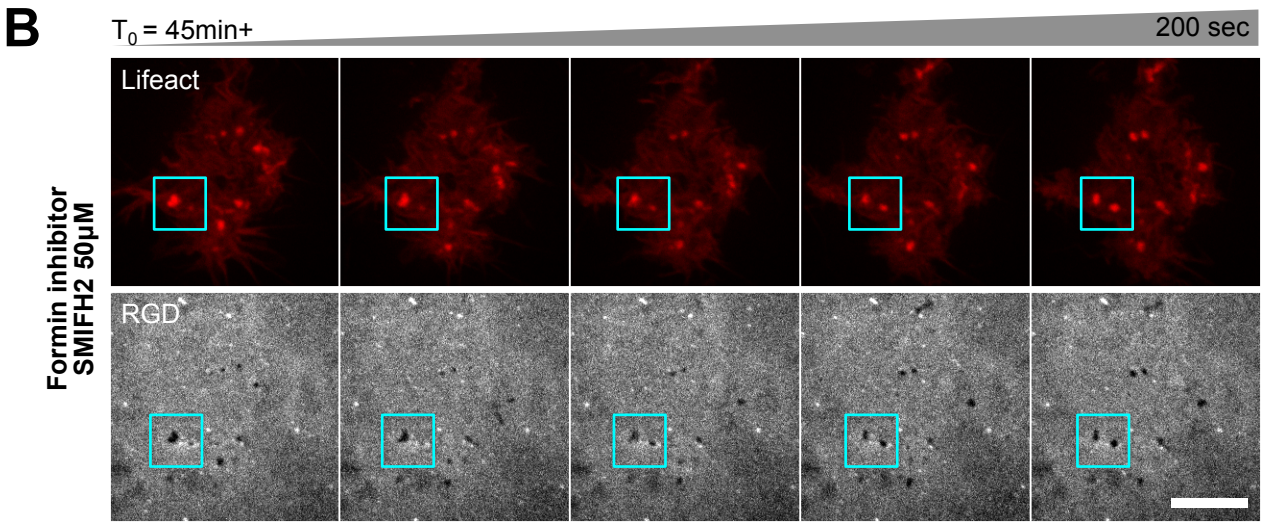

Figure S2. Molecular components at podosomes. (A) Similar to classic podosomes, WIP and cortactin were also recruited at podosome cores when non-transformed fibroblast adhered on RGD membrane. However, formins may not play important roles in F-actin polymerization during podosome formation. mDia1, DAAM1, and FHOD1 formins are not enriched at podosome cores in REF52 fibroblast cells. While mDia1, DAAM1, and FHOD1 were shown to promote linear polymerization of actin in other cellular components, these formins were not enriched at dense F-actin podosome core. Each frame 4x4μm^2. (B) A panformin inhibitor SMIFH2 (50µM, 45min pre-incubation) did not suppress podosome formation in fibroblast cells. Cells were imaged after 45 minutes of initial adhesion. Inside the marked region (cyan squares), podosome formations were able to take place when activities of FH2 domain in formins were inhibited. Scale bar 10µm.

Figure S3. Protrusive dynamics of podosomes.

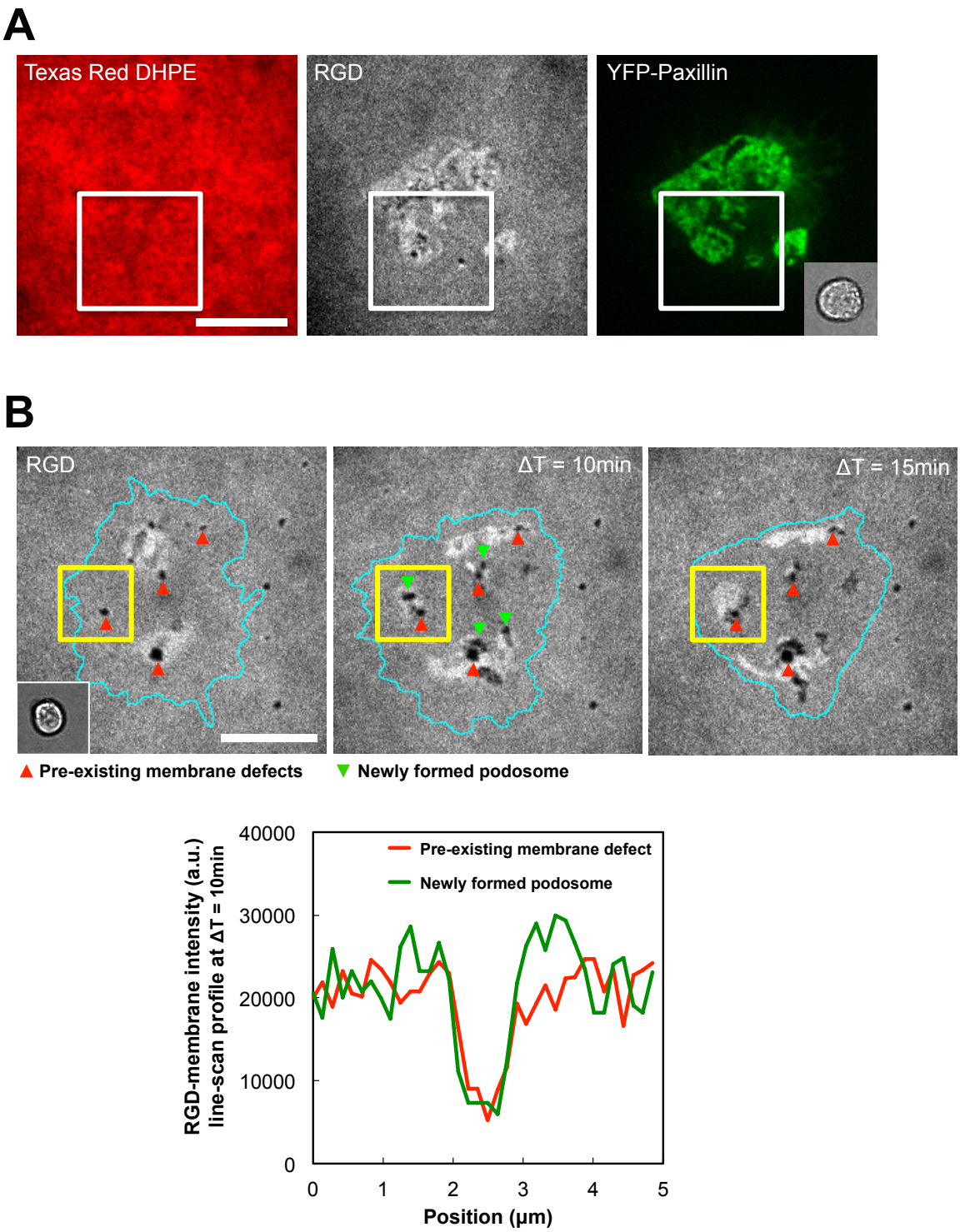

Figure S3. Protrusive dynamics of podosomes. (A) Fluorescent lipid probe Texas Red DHPE (0.1% mol) doped in RGD-membrane remained uniformly distributed during the podosome formation (marked square regions). In spite of the depletion of RGD at podosome core, supported membrane itself stayed continuous without penetration. Inset: bright field image of the cell. (B) REF52 fibroblast cell formed podosomes on RGD-membrane with pre-existing membrane defects (red arrowheads). Membrane defects were due to the imperfection during lipid membrane deposition and were blocked by casein or BSA before the addition of fluorescently labeled neutravidin and RGD. Inside the marked region (yellow squares), a newly formed podosome (green arrowhead) appeared at ΔT= 10min and then disassembled at ΔT= 15min. RGD-membrane intensity line-scan profiles across pre-existing membrane defect (red) and newly formed podosome (green) were examined at ΔT= 10min. The decrease of RGD intensity at podosome core revealed equivalent depletion of RGD, with similar intensity level of the pre-existing membrane defect. Cyan contour indicated cell footprint. Scale bar 10μm.

Figure S4. PI3K and PTEN recruitment at podosomes.

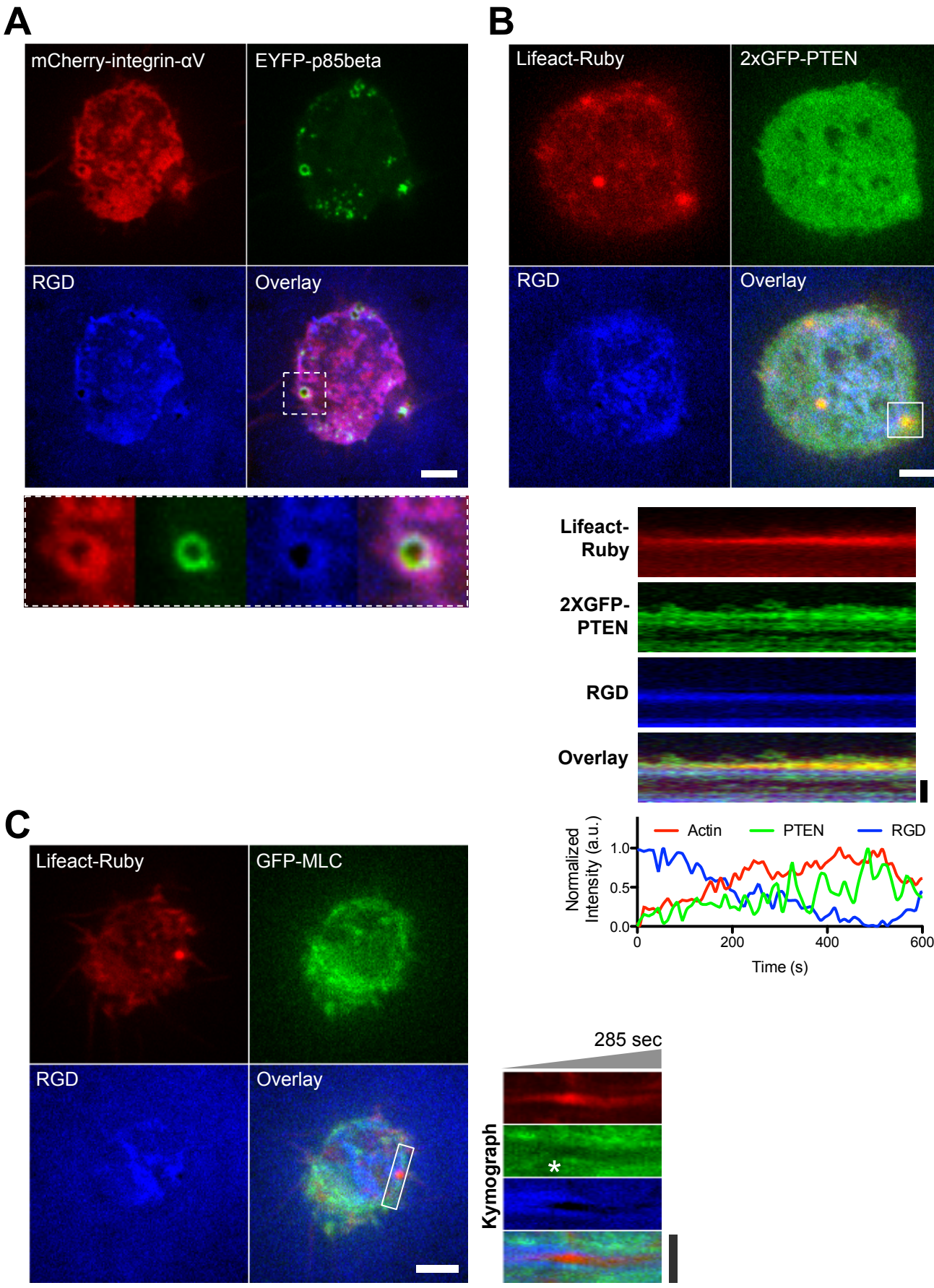

Figure S4. PI3K and PTEN recruitment at podosomes. (A) While mCherry-integrin-αV localized with RGD clusters, p85beta was only recruited at a subset of RGD-integrin clusters, which became podosomes. (B) PTEN was recruited at podosome cores and often found more enriched 500nm above the focal plane of RGD-integrin clusters. Recruitment of 2XGFP-PTEN followed intense F-actin polymerization at podosome core and decreased as F-actin disassembled. (C) Myosin regulatory light chain (MLC) that depicts myosin-II distribution was not enriched at podosomes. The disassembly of podosomes correlated with sparse recruitment of MLC around the dissociating actin core (aster and Movie S3). Scale bar 5μm.

Figure S5. Unaltered PIP3 level at regular focal adhesion.

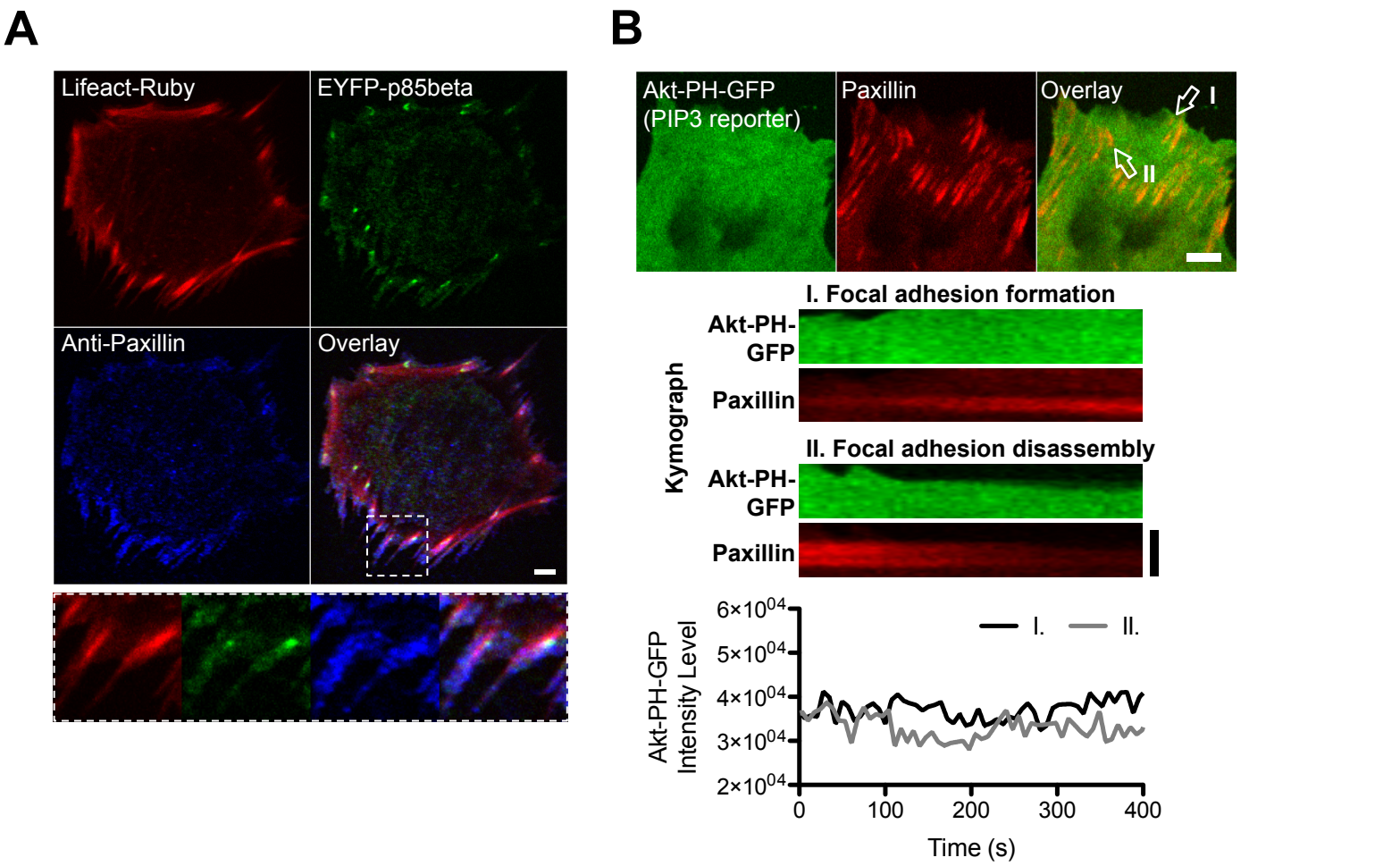

Figure S5. Unaltered PIP3 level at regular focal adhesion. (A) p85beta was found at proximal ends of focal adhesion when cells adhered on RGD-glass. (B) PIP3 levels, monitored by Akt-PH-GFP remains unaltered during focal adhesion assembly (zone I), as well as focal adhesion disassembly (zone II). (C) N-WASP and (D) ARAP3 were not enriched at focal adhesions, which were visualized by paxillin. Scale bar 5μm.

Figure S6. Perturbation of podosome formation by chemical inhibitors.

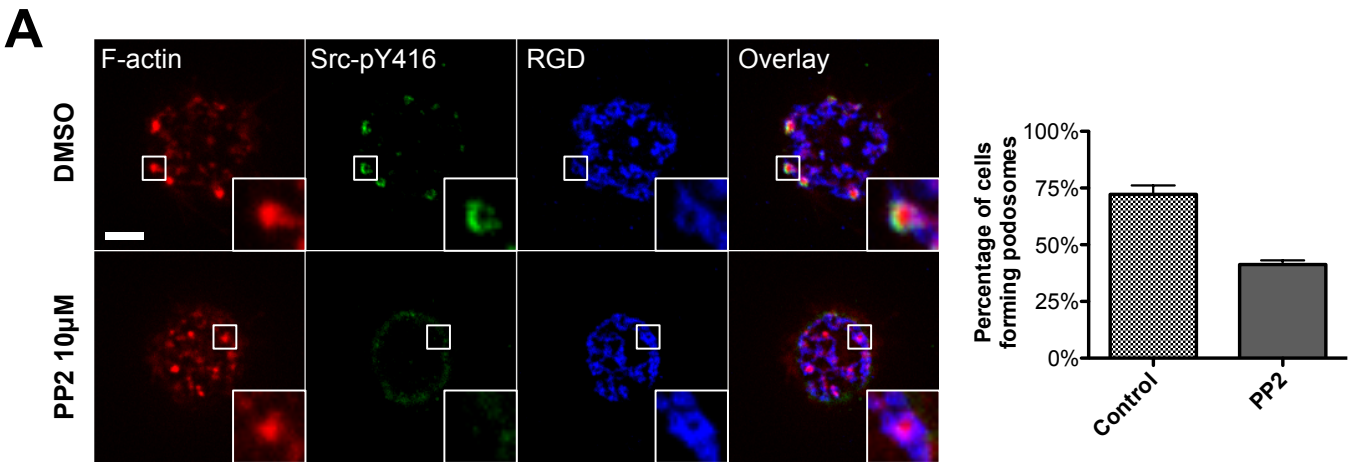

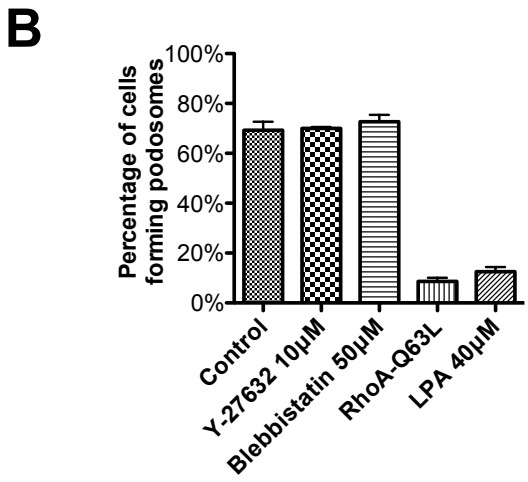

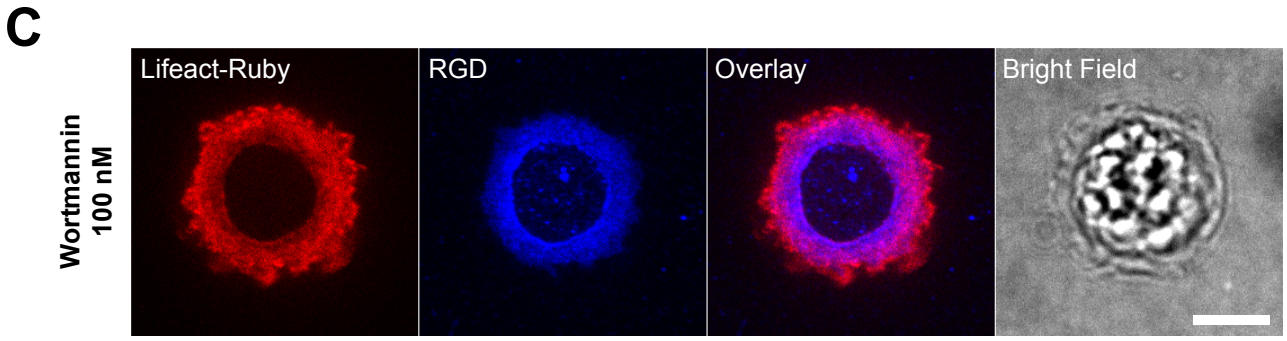

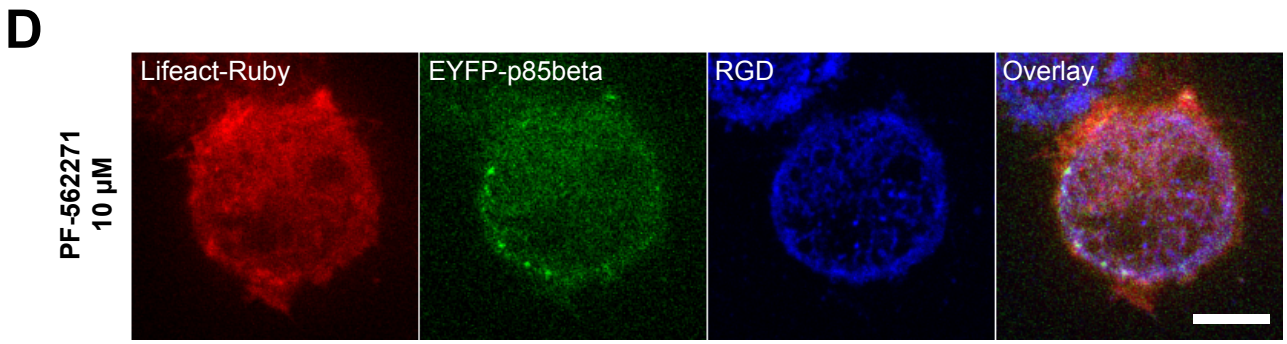

Figure S6. Perturbation of podosome formation by chemical inhibitors. (A) Activated Src kinase was found at podosome ring (overnight Src-pY416 antibody staining). Inhibition of Src by PP2 (10-20μM, 2hr) did not completely block podosome formation. Right panel: approximately 40% of the cells still form podosomes after Src inhibition. Total 104 cells in three experiments. (B) Down-regulation of RhoA-GTP level and inhibition of myosin-II contractility support podosome formation. Percentage of REF52 fibroblast cells forming podosomes under different chemical inhibitors (30min pre-incubation), with SEM from 4 experiments. Y-27632 (10μM) and Blebbistatin (50μM) did not affect podosome formation. LPA (40μM) and constitutively activated RhoA-Q63L mutant effectively abolished podosome formation. (C) and (D) Representative data of fibroblasts on RGD membrane with wortmannin (100nM) and PF-562271 (10μM), respectively. Inhibition of PI3K (wortmannin) and FAK/Pyk2 (PF-562271) both effectively blocked podosome formation. Scale bar 10μm; all error estimates SEM.

Table S1

Podosome component identified:

Podosome core:
F-actin, Arp2/3, WIP, N-WASP (WASP in THP1 macrophages), Cortactin, Cofilin, CapZ beta2, Myosin1E/F, ARAP3, PTEN, Depletion of RGD

Podosome ring:
Integrin/RGD, Talin, Paxillin, Vinculin, Kindlin-1, ILK, FAK, Pyk2, DLC1, FilaminA, Alpha-actinin, VASP, Zyxin, p85beta (from core to ring)

Invadopodia/long-lasting podosome, with constitutively active Src:
MMP-14, Tks5

Supplemental table legend

Table S1. Podosomes were rigorously examined and identified by 1) classic core protein and ring protein components and 2) depletion of RGD intensity inside the RGD ring (Fig. S3B). Podosome formation on RGD-membranes caused ligand exclusion in the podosome core. The RGD intensity at the podosome core was below the level in the rest of the membrane, and recovered after podosomes disassembled (Fig. S3B). Spatial depletion and exclusion of RGD on mobile supported membranes indicated vertical protrusion by local actin assembly. In more than 20 independent experiments with both macrophages and non-transformed fibroblasts, we have extensively verified and confirmed that F-actin polymerization and RGD depletion were always concurrent.

Supplemental movie titles and legends

Movie S1. THP1 monocytic cells formed podosomes on RGD-membranes.
Actin at podosome core was visualized by mCherry-UtrCH. Both GFP-vinculin and RGD were recruited at podosome rings. Scale bar 10μm.

Movie S2. The transition of initial RGD-integrin clusters to podosome.
Podosomes (red arrows) were identified by ring formations of both RGD and YFP-paxillin in the REF52 fibroblast. Scale bar 10μm.

Movie S3. Myosin-II, visualized by MLC-GFP is not enriched at podosome core.
Actin at podosome core was visualized by Lifeact-ruby in RPTPα+/+ mouse fibroblast cells. MLC-GFP was recruited around the dissociating actin core during the disassembly of podosomes. Scale bar 10μm.

Movie S4. Nano-patterned RGD-membranes locally suppress podosome formation.
When a single cell adhered to both a continuous and a partitioned RGD-membrane, podosomes formed only on the continuous region and did not form between the partitioning lines. RGD-membrane with dense nano-partitions impeded podosome formation. Podosomes (red arrows) were identified by ring formations of both RGD and YFP-paxillin in the REF52 fibroblast. Scale bar 10μm.

Movie S5. Spatial-temporal recruitment of p85beta at podosomes.

Class IA PI3K regulatory subunit p85beta was first recruited at pre-podosomal RGD clusters, which was followed by F-actin polymerization in the podosome core. p85beta was subsequently reorganized into podosome rings. Scale bar 10μm.

Movie S6. ARAP3 recruitment at podosomes.

PIP3-bound RhoA-GAP ARAP3 was recruited at podosome cores during F-actin polymerization. Scale bar 10μm.

Supplemental Experimental Procedures

Cell culture and fluorescent fusion proteins. DMEM media, RMPI-1640 media, heat-inactivated fetal bovine serum (HI-FBS), penicillin, streptomycin, HEPES, TrypLE Express (trypsin-like protease), and Neon electroporation kits were purchased from Life Technologies (Grand Island, NY, USA). THP-1 human monocytic leukemia cell line was obtained from Health Protection Agency Culture Collections (Porton Down, Salisbury, UK) and cultured using RPMI-1640 media supplemented with 10% (v/v) HI-FBS and 2 mM glutamine with 50μg/ml 2-Mercaptoethanol (Sigma-Aldrich, St. Louis, MO, USA) in 37 °C incubators with 5% CO_2. THP-1 cells were then stimulated to macrophage-like cells using 1ng/ml human recombinant cytokine TGFβ1 (R&D Systems, Minneapolis, MN, USA) and cultured on glass substrate coated with fibronectin (Sigma-Aldrich, St. Louis, MO, USA). Rat embryonic fibroblast (REF52) and stably expressing YFP-Paxillin REF52 fibroblast and were generous gifts from Dr. Benjamin Geiger, Weizmann Institute of Science, Rehovot, Israel. RPTPα+/+ mouse embryonic fibroblasts(Su et al., 1999) were generous gifts from Dr. Sap JM, NYU, New York, NY, USA. Fibroblast cells were grown in DMEM media supplemented with 10% (v/v) HI-FBS, 100 U/mL penicillin, 100 μg/mL streptomycin, and 20 mM HEPES in 37 °C incubators with 5% CO_2. Podosome formation was observed among all these cell types after 45 minutes of initial adhesion on RGD-membrane.

GFP-talin(Zhang et al., 2008), GFP-N-WASP(Sims et al., 2007), GFP-vinculin(Zamir et al., 1999), FAK-EGFP(Tilghman et al., 2005), Integrin β3-GFP(Ballestrem et al., 2001), MLC-

GFP(Komatsu et al., 2000), Integrin αV-mCherry and mCherry-Paxillin constructs(Kanchanawong et al., 2010), Lifeact-Ruby and Lifeact-GFP (Riedl et al., 2008), mCherry-UtrCH (Burkel et al., 2007) (Addgene 26740), mCherry-Arp3 (Taylor et al., 2011) (Addgene 27682), mCherry-WIP (Cortesio et al., 2010) (Addgene 29573), EYFP-p85beta (Luo et al., 2005) (Addgene 1408), 2XGFP-PTEN (Liu et al., 2005) (Addgene 20739), Akt-PH-GFP (Kwon et al., 2007) (Addgene 18836), EGFP-ARAP3 and EGFP-ARAP3-R982A (Krugmann et al., 2004) (Addgene 39484 and 39487), GFP-DLC1-R677E (Zhong et al., 2009), RhoA FRET biosensor WT and Q63L constitutive mutant (Pertz et al., 2006) (Addgene 12150 and 12151), Constitutive active Src-Y527F (kindly provided by Dr. Keiko Kawauchi, Mechanobiology Institute, Singapore), and MMP-14-mCherry (MT1-MMP) (Steffen et al., 2008) were used to transiently transfect into cells by electroporation (Neon Transfection system, Life Technologies, Grand Island, NY, USA). Fibroblast cells were harvested by TrypLE Express after 18 to 24 hours of transfection. Differentiated THP1 cells were harvested by gentle scrapping after 36-48 hours of transfection. To avoid nonspecific interaction from serum components, cells were then re-suspended in serum-free DMEM media in a 37 °C incubator with 5% CO_2 for 30 min before imaging.

Supported lipid bilayer membranes. 1,2-dioleoyl-*sn*-glycero-3-phosphocholine (DOPC) and 1,2-dipalmitoyl-*sn*-glycero-3-phosphoethanolamine-N-(cap biotinyl) (16:0 biotinyl-Cap-PE) were purchased from Avanti Polar Lipids (Alabaster, AL, USA).

Texas Red 1,2-dihexadecanoyl-sn-glycero-3-phosphoethanolamine, triethylammonium Salt (Texas Red DHPE) was purchased from Life Technologies (Grand Island, NY, USA). Detailed preparation methods were previously described(Lin et al., 2010; Yu et al., 2011). In brief, lipids with a desired composition were mixed in chloroform, and subsequently dried by a rotary evaporator. Mixed lipids were then hydrated with 2mL of DI water over night. Small lipid vesicles, usually 100nm in diameter, were made by 60-second probe-sonication in an ice bath, and then centrifuged at 20000G for 4-hour. 1mL of supernatant solution of small lipid vesicles was collected and stored at 4°C. Glass substrates were cleaned by bath-sonication in 1:1 (V/V) isopropyl alcohol: water mixture for 30-minute and rinsed with 50mL DI water 10 times. Glass substrates were immersed in 50% sulfuric acid overnight (Caution!! Avoid eye and skin exposure) and then rinsed with 50mL DI water 10 times. Before membrane deposition, glass substrates were then exposed to intense deep-UV (185nm) in an enclosed container for 30-minute (Caution!! Avoid eye and skin exposure), rinsed with 50mL DI water 10 times, and dried under a nitrogen gas stream. The lipids (0.2 mol% of biotinyl-Cap-PE and 99.8 mol% of DOPC) were mixed with an equal volume of 1x PBS, and then pipetted onto cleaned glass substrates for the self-assembly processes. When needed, 0.2% of Texas Red DHPE (mole% of DOPC) was used to monitor the integrity of supported membrane. Excess lipid vesicles were removed by immersing the entire glass substrate into a DI water bath. The lipid-coated glass substrate was then assembled with an Attofluor cell chamber (Life Technologies, Grand Island, NY, USA) or Chamlide magnetic chamber (Live Cell Instrument, Seoul, Korea) within the water bath at room temperature. After

assembly, supported lipid membranes in the chamber were always kept under aqueous conditions by immersing with 2mL of solvent.

Membrane functionalization. Supported lipid membrane was first blocked by incubation of 10-50μg/mL of bovine serum albumin (BSA) or casein (Sigma-Aldrich, St. Louis, MO, USA) for 30-minute, in order to passivate metal surface of nano-patterned lines. Excess blocking solution was removed by serial solvent exchange, 25mL of 1x PBS in total for each chamber. 0.1μg/mL of Cascade Blue neutravidin (Life Technologies, Grand Island, NY, USA) or DyLight 680 neutravidin (Thermo Fisher Scientific Inc., Rockford, IL, USA) was added onto supported lipid membranes for 30-minute in room temperature. Neutravidin serves as the link between biotinyl-Cap-PE and biotinylated RGD peptide. Excess neutravidin was removed by serial solvent exchange, 25mL of PBS in each chamber. Next, 1μg/mL of biotinylated RGD, *cyclo* [Arg-Gly-Asp-D-Phe-Lys(Biotin-PEG-PEG)](Peptides International Inc., Louisville, KY, USA), was added to neutravidin-coated supported membranes for 30-minute in room temperature. Excess RGD was removed by serial solvent exchange, 25mL of 1x PBS in each chamber, and then 15mL of serum-free DMEM media. Live cells were then added onto RGD-functionalized supported membranes within 2-hour after preparation. Based on quantitative fluorescence calibration(Salaita et al., 2010), the surface density of biotinylated RGD linked by neutravidin on 0.2mol% biotin-lipid membranes was approximately 900 ± 200 molecules/μm^2.

Immunofluorescence and inhibition chemicals. For fixed cell experiments, cells were fixed with 4% flesh-prepared paraformaldehyde, permeabilized with 0.05% Triton X, blocked with 5% casein overnight. Phalloidin labeled with CF405, CF594, and CF680R dye were purchased from Biotium (Hayward, CA, USA). Phospho-FAK Tyr397 monoclonal antibody (31H5L17) and paxillin monoclonal antibody (5H11) were purchased from Life Technologies (Grand Island, NY, USA). Tks5 polyclonal antibody (SH3 #1, 09-403) was purchased from EMD Millipore (Billerica, MA, USA). Phospho-Src family (Tyr416) polyclonal antibody (#2101) was purchased from Cell Signaling (Boston, MA, USA). Anti-FLAG monoclonal antibody (M2), blebbistatin, Y-27632, oleoyl-L-α-lysophosphatidic acid sodium salt (LPA), SMIFH2, and PP2 were purchased from Sigma-Aldrich (St. Louis, MO, USA). Wortmannin and PF-562271 were purchased from Selleck Chemicals. (Houston, TX, USA). Chemicals were first kept as a stock concentration 1000-times higher than the final concentration. Before applying to cells, chemicals were diluted 1000-times into DMEM media.

Microscopy and data analyses. Fluorescent images of live cells were taken by an inverted spinning-disk confocal microscope (PerkinElmer UltraVIEW VoX, Waltham, MA, USA), with 100x oil immersion lens (1.40 NA, UPlanSApo 100x, Olympus, Center Valley, PA, USA) and cooled EMCCD camera (C9100-13, Hamamatsu Photonics, Hamamatsu, Japan). An environmental chamber (37°C and 5% CO_2) was attached to the microscope body for long-term time-lapse imaging. Filter cube of 530/11nm excitation and 50/50 beam-splitter as dichroic mirror was used to perform interference reflection microscopy (IRM). For RhoA FRET biosensor imaging, FRET channel channel was monitored by

440nm laser excitation and 587/125nm emission filter. CFP channel was monitored by 440nm laser excitation with 485/60nm emission filter and was used as the reference baseline. The camera parameters and microscope settings were kept fixed, in order to cross-compare different cells. Acquired images were analyzed by ImageJ (NIH, Bethesda, MD, USA). For the FRET analysis, background in each channel was first measured and manually subtracted(Pertz et al., 2006). Boundary of each cell was then defined by image threshold in YFP channel, and regions outside of the cell boundary in FRET channel was set to zero value. The imaging-based FRET efficiency was measure of the ratio between corrected FRET channel and YFP channel. Statistical testing was analyzed by Igor Pro (WaveMetrics, Inc., Portland, OR, USA). Two-sample T-tests were performed, and *p*-value was calculated under the condition of two-tailed distribution and alpha=0.05. Statistical bar graphs with mean and standard error of the mean (SEM) were plotted by Prism (GraphPad Software, Inc., La Jolla, CA, USA).

Supplemental References

Ballestrem, C., Hinz, B., Imhof, B.A., and Wehrle-Haller, B. (2001). Marching at the front and dragging behind. J Cell Biol *155*, 1319-1332.

Burkel, B.M., von Dassow, G., and Bement, W.M. (2007). Versatile fluorescent probes for actin filaments based on the actin-binding domain of utrophin. Cell motility and the cytoskeleton *64*, 822-832.

Cortesio, C.L., Perrin, B.J., Bennin, D.A., and Huttenlocher, A. (2010). Actin-binding protein-1 interacts with WASp-interacting protein to regulate growth factor-induced dorsal ruffle formation. Molecular biology of the cell *21*, 186-197.

Kanchanawong, P., Shtengel, G., Pasapera, A.M., Ramko, E.B., Davidson, M.W., Hess, H.F., and Waterman, C.M. (2010). Nanoscale architecture of integrin-based cell adhesions. Nature *468*, 580-584.

Komatsu, S., Yano, T., Shibata, M., Tuft, R.A., and Ikebe, M. (2000). Effects of the regulatory light chain phosphorylation of myosin II on mitosis and cytokinesis of mammalian cells. The Journal of biological chemistry *275*, 34512-34520.

Krugmann, S., Williams, R., Stephens, L., and Hawkins, P.T. (2004). ARAP3 is a PI3K- and rap-regulated GAP for RhoA. Current biology : CB *14*, 1380-1384.

Kwon, Y., Hofmann, T., and Montell, C. (2007). Integration of phosphoinositide- and calmodulin-mediated regulation of TRPC6. Molecular cell *25*, 491-503.

Lin, W.-C., Yu, C.-H., Triffo, S., and Groves, J.T. (2010). Supported Membrane Formation, Characterization, Functionalization, and Patterning for Application in Biological Science and Technology (John Wiley & Sons, Inc.).

Liu, F., Wagner, S., Campbell, R.B., Nickerson, J.A., Schiffer, C.A., and Ross, A.H. (2005). PTEN enters the nucleus by diffusion. Journal of cellular biochemistry *96*, 221-234.

Luo, J., Field, S.J., Lee, J.Y., Engelman, J.A., and Cantley, L.C. (2005). The p85 regulatory subunit of phosphoinositide 3-kinase down-regulates IRS-1 signaling via the formation of a sequestration complex. J Cell Biol *170*, 455-464.

Pertz, O., Hodgson, L., Klemke, R.L., and Hahn, K.M. (2006). Spatiotemporal dynamics of RhoA activity in migrating cells. Nature *440*, 1069-1072.

Riedl, J., Crevenna, A.H., Kessenbrock, K., Yu, J.H., Neukirchen, D., Bista, M., Bradke, F., Jenne, D., Holak, T.A., Werb, Z*., et al.* (2008). Lifeact: a versatile marker to visualize F-actin. Nat Meth *5*, 605-607.

Salaita, K., Nair, P.M., Petit, R.S., Neve, R.M., Das, D., Gray, J.W., and Groves, J.T. (2010). Restriction of receptor movement alters cellular response: physical force sensing by EphA2. Science *327*, 1380-1385.

Sims, T.N., Soos, T.J., Xenias, H.S., Dubin-Thaler, B., Hofman, J.M., Waite, J.C., Cameron, T.O., Thomas, V.K., Varma, R., Wiggins, C.H*., et al.* (2007). Opposing effects of PKCtheta and WASp on symmetry breaking and relocation of the immunological synapse. Cell *129*, 773-785.

Steffen, A., Le Dez, G., Poincloux, R., Recchi, C., Nassoy, P., Rottner, K., Galli, T., and Chavrier, P. (2008). MT1-MMP-dependent invasion is regulated by TI-VAMP/VAMP7. Current biology : CB *18*, 926-931.

Su, J., Muranjan, M., and Sap, J. (1999). Receptor protein tyrosine phosphatase alpha activates Src-family kinases and controls integrin-mediated responses in fibroblasts. Current biology : CB *9*, 505-511.
Taylor, M.J., Perrais, D., and Merrifield, C.J. (2011). A high precision survey of the molecular dynamics of mammalian clathrin-mediated endocytosis. PLoS biology *9*, e1000604.
Tilghman, R.W., Slack-Davis, J.K., Sergina, N., Martin, K.H., Iwanicki, M., Hershey, E.D., Beggs, H.E., Reichardt, L.F., and Parsons, J.T. (2005). Focal adhesion kinase is required for the spatial organization of the leading edge in migrating cells. Journal of cell science *118*, 2613-2623.
Yu, C.H., Law, J.B., Suryana, M., Low, H.Y., and Sheetz, M.P. (2011). Early integrin binding to Arg-Gly-Asp peptide activates actin polymerization and contractile movement that stimulates outward translocation. Proceedings of the National Academy of Sciences of the United States of America *108*, 20585-20590.
Zamir, E., Katz, B., Aota, S., Yamada, K., Geiger, B., and Kam, Z. (1999). Molecular diversity of cell-matrix adhesions. Journal of cell science *112*, 1655-1669.
Zhang, X., Jiang, G., Cai, Y., Monkley, S.J., Critchley, D.R., and Sheetz, M.P. (2008). Talin depletion reveals independence of initial cell spreading from integrin activation and traction. Nat Cell Biol *10*, 1062-1068.
Zhong, D., Zhang, J., Yang, S., Soh, U.J., Buschdorf, J.P., Zhou, Y.T., Yang, D., and Low, B.C. (2009). The SAM domain of the RhoGAP DLC1 binds EF1A1 to regulate cell migration. Journal of cell science *122*, 414-424.